A PORTABLE GAS-FILTER-CORRELATION SPECTROMETER FOR HCl AND HF

SCIENCE APPLICATIONS, INCORPORATED

PREPARED FOR
SCHOOL OF AEROSPACE MEDICINE

OCTOBER 1975

Report SAM-TR-75-33

A PORTABLE GAS-FILTER-CORRELATION SPECTROMETER FOR HCl AND HF

Science Applications, Inc.
La Jolla, California 92038

October 1975

Final Report for Period 15 January 1974 - 31 January 1975

Prepared for
USAF SCHOOL OF AEROSPACE MEDICINE
Aerospace Medical Division (AFSC)
Brooks Air Force Base, Texas 78235

NOTICES

This final report was submitted by Science Applications, Inc., La Jolla, California 92037, under contract F41608-74-C-0018, with the USAF School of Aerospace Medicine, Aerospace Medical Division, AFSC, Brooks Air Force Base, Texas, under job order 7184-18-08. Dr. Richard L. Miller (VNL) was the Laboratory Project Scientist-in-Charge.

When U.S. Government drawings, specifications, or other data are used for any purpose other than a definitely related Government procurement operation, the Government thereby incurs no responsibility nor any obligation whatsoever; and the fact that the Government may have formulated, furnished, or in any way supplied the said drawings, specifications, or other data is not to be regarded by implication or otherwise, as in any manner licensing the holder or any other person or corporation, or conveying any rights or permission to manufacture, use, or sell any patented invention that may in any way be related thereto.

This report has been reviewed by the Information Office (OI) and is releasable to the National Technical Information Service (NTIS). At NTIS, it will be available to the general public, including foreign nations.

This technical report has been reviewed and is approved for publication.

RICHARD L. MILLER, Ph.D.
Project Scientist

E. G. SHAW, Ph.D.
Supervisor

ROBERT G. McIVER, Colonel, USAF, MC
Commander

UNCLASSIFIED

SECURITY CLASSIFICATION OF THIS PAGE (When Data Entered)

REPORT DOCUMENTATION PAGE		READ INSTRUCTIONS BEFORE COMPLETING FORM
1. REPORT NUMBER SAM-TR-75-33	2. GOVT ACCESSION NO.	3. RECIPIENT'S CATALOG NUMBER
4. TITLE (and Subtitle) A PORTABLE GAS-FILTER-CORRELATION SPECTROMETER FOR HCl AND HF		5. TYPE OF REPORT & PERIOD COVERED Final Report-- 15 Jan. 1974 to 31 Jan. 1975 6. PERFORMING ORG. REPORT NUMBER SAI-75-525-LJ
7. AUTHOR(s) E. Roy Bartle		8. CONTRACT OR GRANT NUMBER(s) F41609-74-C-0014
9. PERFORMING ORGANIZATION NAME AND ADDRESS Science Applications, Inc. 1200 Prospect Street La Jolla, California 92038		10. PROGRAM ELEMENT, PROJECT, TASK AREA & WORK UNIT NUMBERS 62202F 7164-16-09
11. CONTROLLING OFFICE NAME AND ADDRESS USAF School of Aerospace Medicine (VNL) Aerospace Medical Division (AFSC) Brooks Air Force Base, Texas 78235		12. REPORT DATE October 1975 13. NUMBER OF PAGES 41
14. MONITORING AGENCY NAME & ADDRESS (if different from Controlling Office)		15. SECURITY CLASS. (of this report) Unclassified 15a. DECLASSIFICATION/DOWNGRADING SCHEDULE

16. DISTRIBUTION STATEMENT (of this Report)

Approved for public release; distribution unlimited.

17. DISTRIBUTION STATEMENT (of the abstract entered in Block 20, if different from Report)

PRICES SUBJECT TO CHANGE

18. SUPPLEMENTARY NOTES

19. KEY WORDS (Continue on reverse side if necessary and identify by block number)

Toxic-vapor detection
Gas-filter-correlation
Remote sensing

20. ABSTRACT (Continue on reverse side if necessary and identify by block number)

A portable gas-filter-correlation spectrometer (GFCS) has been developed to continuously monitor HCl and HF over the concentration range from 0.2 to 1000 ppm. The unit operates using either 115 VAC 60 Hz or 12 VDC. The attained threshold sensitivities of 167 and 200 ppb for HCl and HF, respectively, are nearly those predicted from theoretical considerations. Excellent specificity is obtained in the presence of anticipated interfering species. The system also can be converted into an active long-path system using a

DD FORM 1 JAN 73 1473 EDITION OF 1 NOV 65 IS OBSOLETE

UNCLASSIFIED

20. ABSTRACT (Continued)

retroreflector; ranges up to 500 m (1-km optical path) can be used with about the same sensitivities. A technique for passive single-ended remote sensing is described that appears to offer significant potential for ranges up to 1 km

CONTENTS

LIST OF FIGURES

LIST OF TABLES

A PORTABLE GAS-FILTER-CORRELATION SPECTROMETER FOR HCl AND HF

INTRODUCTION

The need to develop improved techniques for monitoring HCl and HF in the ambient air has been clearly established. The same need, in fact, exists for many air pollutants.

Some instruments (electrochemical transducers, chromatographs, dispersive and nondispersive spectrometers, and lasers) are being used or developed to monitor air pollutants. However, a recent review article in Science (9) points out that most instruments presently being used for air pollutant monitoring are based on wet chemical analyses. While these instruments have demonstrated utility, they suffer severe drawbacks such as (1) interferences by other pollutants and naturally occurring atmospheric species, (2) instability of the chemicals, (3) complex plumbing, (4) difficulty in unattended, routine operation, (5) difficulty in real-time measurements, and (6) severe problems related to sampling (9).

These difficulties have spurred intensive development of analytical techniques based upon the physical properties of pollutants (9, 10). In 1968, Science Applications, Inc. (SAI) personnel investigated the possibility of remotely detecting global air pollution from satellites (5). They concluded that measuring the spectral absorption of electromagnetic energy by pollutants would provide a means to remotely monitor the pollutants; however, very high sensitivity and specificity (freedom from interference) requirements would be imposed upon the sensors.

Since 1969, SAI personnel have been developing remote sensors for the National Aeronautics and Space Administration that satisfy the sensitivity and specificity requirements (7). These sensors are based upon the principle of gas filter correlation (GFC). Two instruments have been built and test flown (6). Furthermore, SAI has developed remote GFC SO_2 sensors for the Environmental Protection Agency (1, 2).

The potential of the GFC technique for remotely detecting air pollutants led to establishing its feasibility for in-situ monitoring of such pollutants. Basic laboratory experiments have indeed shown that a high-sensitivity and -specificity instrument can be developed (3).

This report presents the theoretical development of a GFC spectrometer for measuring both HCl and HF, the detailed design of the spectrometer, the results of laboratory testing, a discussion of the test results, and conclusions and recommendations.

A System Equipment Manual describing the specifications, operation, calibration, and maintenance of the spectrometer is provided separately from this report.

THEORETICAL DESCRIPTION OF GAS-FILTER-CORRELATION SPECTROMETRY

Background

Infrared absorption spectroscopy has long served as a powerful technique for gas mixture analysis. In contrast to dispersive spectroscopy, a nondispersive infrared (NDIR) device makes use of the particular gas to provide specificity.

Luft (8) gave the first detailed description of an NDIR instrument--using two different light sources; two cells; and one membrane condenser, sensitized with the gas of interest, as a detector. This method, using a sensitized detector and the gas sample in one light beam, was later classified as "positive filtering."

A different arrangement by Wright and Herscher (11) used one light source, two cells, and two detectors which were the two opposed arms of an AC-excited bolometer. In this case, the selectivity was provided by balancing the two cells, and the detectors were nonselective. The gas sample was introduced into a cell common to both light beams. This was later classified as "negative filtering."

Since 1969, SAI personnel have been developing sensors based on NDIR (1-3, 6, 7). If the optical thickness of the comparison gas in the sensor is kept small, an ultimate high-spectral-resolution filter (provided by the natural line-width of the gas) results. High spectral resolution is the most important parameter in obtaining specificity and accuracy in pollutant analysis. The term "gas filter correlation" (GFC) was adopted to describe the sensors using this technique.

GFC is based upon absorption or emission of electromagnetic energy by the specific pollutant to be monitored. As such, GFC can operate in the UV, visible, or IR regions of the spectrum. The IR may

be preferable because all pollutants of interest have rotational lines that absorb in the IR; also, scattering effects are more pronounced in the UV and visible. On the other hand, the UV-visible may be preferable if extreme spectral interferences occur in the IR; also, more sensitive photomultiplier detectors are available and pollutant absorptivities are greater.

Conventional spectroscopic instruments depend upon finding a single absorption line of a particular species. GFC uses the contribution of all absorption lines of a particular species' band system.

Specificity is obtained by using random correlation between spectra arising from the particular and the interfering species; the principle of random correlation has been established (3, 6) for most pollutant species and for interfering species occurring naturally and in polluted atmospheres. In addition, a ratioing technique may be used that minimizes effects of source intensity changes, background radiation, and continuum absorption due to complex molecules, aerosols, or water vapor.

The GFC technique can be applied to both double- and single-ended systems. For the double-ended system, an active infrared source and GFC receiver are used to measure an intervening pollutant; in this case, the detection principle is based upon absorption spectroscopy. For the single-ended system, only the GFC receiver is used to remotely detect a pollutant; in this case, the detection principle is based upon either emission or absorption spectroscopy, depending upon the relative temperatures of the pollutant to be detected and the background.

Analysis of Double-Ended GFC Technique

A schematic diagram which illustrates the technique is presented in Figure 1. The basic components are a high-temperature infrared source; a sample cell in which the gas mixture to be analyzed is placed; a rotating chopper; a reference cell containing a vacuum or a transparent gas such as nitrogen; a specifying cell containing a sample of the gas to be detected; an adjustable aperture limiting the radiation passing through the reference cell; an optical filter confining the radiation to the spectral region where the gas to be detected possesses absorption bands; a sensitive infrared detector; and optics to collimate the radiance from the source and to focus it on the detector. The radiation from the source passes through the sample cell where it is spectrally absorbed by the specific gas and all possible interfering gases. The radiation, having traversed the sample cell, is alternately passed through the reference and specifying cells. When passing through the reference cell, the radiation

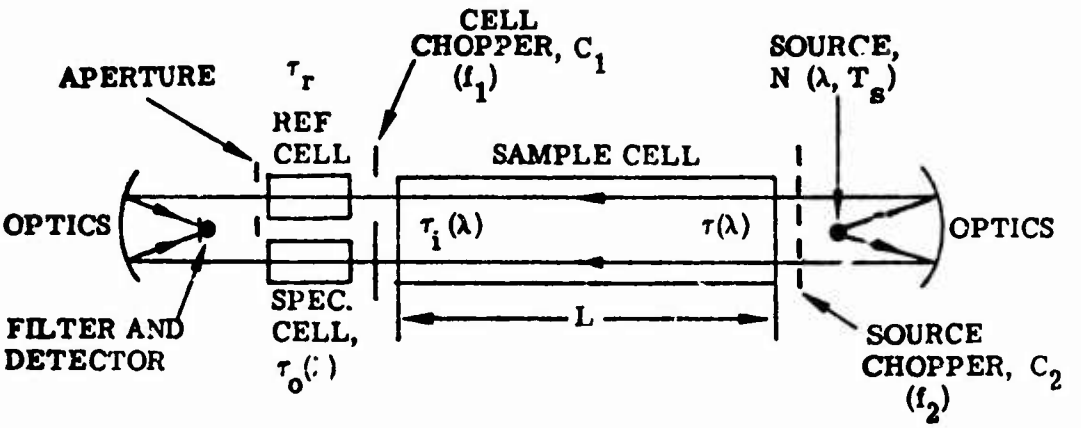

Figure 1. Schematic diagram of double-ended GFC technique.

is unattenuated; but when passing through the specifying cell, it is attenuated by the spectral absorption character of the gas in the cell. Thus, an alternating signal is generated at the detector. The magnitude of this signal is related to the concentration of the gas to be detected in the sample cell.

The following development assumes that self-emission by the sample gas is negligible compared with the source radiance, N. Referring to Figure 1, when the cell chopper at frequency f_1 is in the position indicated, the energy from the source which reaches the detector through the reference cell is given by

$$E_1 = \int_{\Delta\lambda} C(\lambda)\, N(\lambda, T_s)\, \tau_i(\lambda)\, \tau(\lambda)\, \tau_r\, d\lambda \qquad (1)$$

where

$C(\lambda)$	is the spectral attenuation due to the optics, cell windows, and optical filter;
$N(\lambda, T_s)$	is the radiance from the source;
$\tau_i(\lambda)$	is the spectral transmission through possible interfering gases;
$\tau(\lambda)$	is the spectral transmission due to the gas to be detected;
τ_r	is the transmission through the aperture.

E is obtained by integrating over the spectral wavelength interval $\Delta\lambda$ defined by the optical filter. Radiation, due to self-emission by the gases, windows, and other instrument components, is neglected, since for source temperatures greater than 1000°K and wavelengths less than 5 μm, the radiance from the source is at least three orders of magnitude greater than the radiance from 300°K materials.

Similarly, when the cell chopper passes radiation through the specifying cell, the energy reaching the detector is given by

$$E_2 = \int_{\Delta\lambda} C'(\lambda)\, N(\lambda, T)\, \tau_i(\lambda)\, \tau(\lambda)\, \tau_o(\lambda) d\lambda \qquad (2)$$

where $\tau_o(\lambda)$ is the transmission due to the gas in the specifying cell and $C'(\lambda)$ is the spectral attenuation due to the optics.

The peak-to-peak signal difference at the detector by chopping is proportional to the difference between E_2 and E_1; that is,

$$\Delta V \alpha E_2 - E_1 = \int_{\Delta\lambda} N(\lambda, T)\, \tau_i(\lambda)\, \tau(\lambda) \left[C'(\lambda)\, \tau_o(\lambda) - C(\lambda)\, \tau_r \right] d\lambda \qquad (3)$$

Now, for slowing varying functions in λ, $N(\lambda, T_s)$ and $C'(\lambda)$ can be averaged over the interval $\Delta\lambda$. Thus,

$$\Delta V \alpha \bar{N}\, \bar{C}' \int_{\Delta\lambda} \tau_i(\lambda)\, \tau(\lambda) \left[\tau_o(\lambda) - \frac{C(\lambda)}{C'(\lambda)}\, \tau_r \right] d\lambda \qquad (4)$$

where the bars indicate mean values over $\Delta\lambda$. But, $\tau_o(\lambda)$ and $\tau(\lambda)$ are strongly correlated, since they represent the spectral transmission due to the same gas, and $\tau_i(\lambda)$ is assumed to be uncorrelated with $\tau_o(\lambda)$. Then, applying the mean value theorem,

$$\Delta V \alpha \bar{N}\, \bar{C}'\, \bar{\tau}_i \left[\overline{\tau \tau_o} - (\overline{C/C'})\, \bar{\tau}\, \tau_r \right] \Delta\lambda \qquad (5)$$

Since the two parameters $C(\lambda)$ and $C'(\lambda)$ differ from each other by only very minor differences between the nominally identical optical paths, the product of their ratio and the instrument adjustable aperture transmission may be considered to be an effective aperture, τ_r'. Thus,

$$\Delta V = K \bar{N} \bar{\tau}_i \left[\overline{\tau \tau}_o - \bar{\tau} \tau'_r \right] \tag{6}$$

for a given set of instrument parameters, where K is a proportionality constant.

To zero the instrument, the optical path is made transparent ($\tau = \tau_i = 1$) and the aperture adjusted such that $\tau'_r = \tau_o$. Thus,

$$\Delta V = K \bar{N} \left[\overline{\tau \tau}_o - \bar{\tau} \bar{\tau}_o \right] = K \bar{N} M \tag{7}$$

where M is the AC modulation.

As seen from Equation 5, the instrument signal, ΔV, may be increased by increasing the source radiance, $\bar{N}$, and by judicious selection of the transmission through the specifying cell, $\bar{\tau}_o$.

From this development, ΔV is proportional to $\bar{N}$, $\bar{\tau}_i$, and the overall responsivity and efficiency of the instrument. To eliminate these dependencies, a double-chopper system is used to facilitate an electronic ratioing technique. The signals generated by this system are shown schematically in Figure 2.

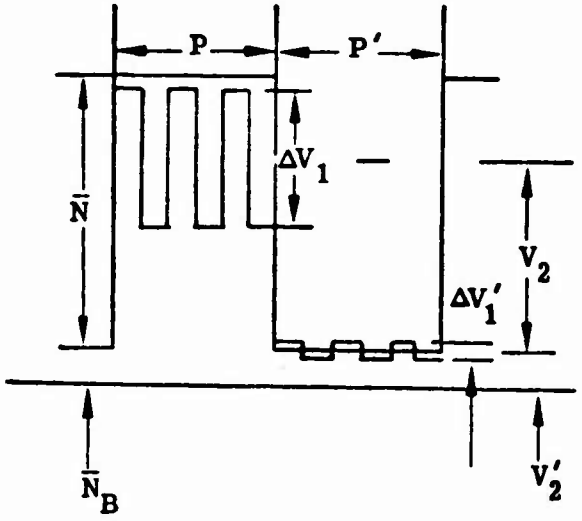

Figure 2. Schematic diagram of signals generated by double-chopping GFC instrument.

Here we assume the source chopper, C_2, is operating at a lower frequency (f_2) than the instrument cell chopper, C_1. And we assume all background radiation, from the instrument or extraneous, is contained in the single term "$\bar{N}_B$." Then, the signals generated at frequency f_1 during phase P are given by

$$\Delta V_1 = (\bar{N} + \bar{N}_B)(\overline{\tau\tau}_o - \bar{\tau}\tau_r) + \bar{N}_{C_1}(\tau_r - \bar{\tau}_o) \tag{8}$$

where $\bar{N}_{C_1}$ is the radiance from chopper C_1 and the remaining symbols are as previously defined.

Similarly, during phase P′, when the source is blocked,

$$\Delta V_1' = (\bar{N}_B + \bar{N}_{C_2})(\overline{\tau\tau}_o - \bar{\tau}\tau_r) + \bar{N}_{C_1}(\tau_r - \bar{\tau}_o) \tag{9}$$

Now, $\Delta V_1 >> \Delta V_1'$, being proportional to the source radiance, so $\Delta V_1'$ is easily subtracted electronically from ΔV_1, giving

$$S_1 = \Delta V_1 - \Delta V_1' = (\bar{N} - \bar{N}_{C_2})(\overline{\tau\tau}_o - \bar{\tau}\tau_r) \tag{10}$$

The result is an AC signal at frequency f_1

The signals at frequency f_2 are similarly obtained. During P,

$$V_2 = (\bar{N} + \bar{N}_B)\left(\frac{\overline{\tau\tau}_o + \bar{\tau}\tau_r}{2}\right) + \bar{N}_{C_1}\left(\frac{\bar{\tau}_o + \tau_r}{2}\right) \tag{11}$$

and during P′,

$$V_2' = (\bar{N}_B + \bar{N}_{C_2})\left(\frac{\overline{\tau\tau}_o + \bar{\tau}\tau_r}{2}\right) + \bar{N}_{C_1}\left(\frac{\bar{\tau}_o + \tau_r}{2}\right) \tag{12}$$

Subtracting gives

$$S_2 = V_2 - V_2' = (\bar{N} - \bar{N}_{C_2})\left(\frac{\overline{\tau\tau}_o + \bar{\tau}\tau_r}{2}\right) \tag{13}$$

Forming the ratio between Equations 10 and 13 yields

$$\frac{S_1}{S_2} = 2\left(\frac{\overline{\tau\tau}_o - \bar{\tau}\tau_r}{\overline{\tau\tau}_o + \bar{\tau}\tau_r}\right) \tag{14}$$

This ratio is completely independent of all temperature-dependent instrument parameters, being a function only of the unknown transmissivity $\bar{\tau}$ and the instrument transmissivities $\bar{\tau}_o$ and τ_r. Thus, an extremely stable (no drift) signal results.

Analysis of Single-Ended Remote GFC Technique

The RGFC technique is used for remote, passive detection of pollutants. In this case the problem of measuring pollutants quantitatively is more complex. To illustrate the problem, consider a sensor receiving energy from a polluted cloud or plume with a cold sky as the background (see Fig. 3).

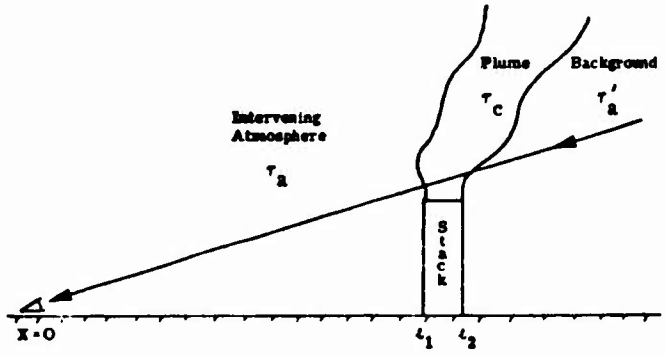

Figure 3. Schematic of viewing geometry.

The phenomenology for remote detection of pollutants depends upon specific spectral measurements of infrared radiation. From the basic

theory of radiative transfer (4), an expression is developed which describes the monochromatic radiation received by the sensor from the background (emission of the atmosphere from infinity to the far edge of the plume), the effluent plume (emission of the plume), and the intervening atmosphere (emission of the atmosphere between the plume and the sensor).

$$E(\lambda) = \tau_c \tau_a \int_{\infty}^{\ell_2} N_b^o [T_b(x)] \frac{\partial \tau_a'(x)}{\partial x} dx + \tau_a \int_{\ell_2}^{\ell_1} N_c^o [T_c(x)] \frac{\partial \tau_c(x)}{\partial x} dx + \int_{\ell_1}^{o} N_b^o [T_b(x)] \frac{\partial \tau_a}{\partial x} dx \quad (15)$$

$N^o[T(x)]$ represents the blackbody function at temperature T, which is, in general, a function of x along the line of sight and, of course, also a function of wavelength λ. The atmospheric transmission is indicated by the terms τ_a and τ_a'; it consists of the transmissivities of all normal atmospheric species; i.e.,

$$\tau_a = \tau(CO_2) \times \tau(H_2O) \times \tau(CH_4) \times \tau(N_2O)... \quad (16)$$

The transmissivity of the plume is similarly formulated

$$\tau_c = \tau \times \tau(CO_2) \times \tau(H_2O) \times \tau(N_2O) \times \tau(CH_4)... \quad (17)$$

This may be written as $\tau_c = \tau \tau_i$, where τ is the transmissivity due to the pollutant and τ_i is the transmissivity of all interfering species. The general expression for transmissivity is given by

$$\tau = \exp - \int_{\ell_2}^{\ell_1} k(\lambda) C(x) p_t(X) dx \quad (18)$$

where $k(\lambda)$ is the spectral absorption coefficient of the pollutant, C is the unknown concentration in the plume, and p_t is the total pressure of the plume.

Equations 15-18 show that the task of quantifying the pollutant concentration in the plume is complex. The radiation received by the sensor is a function of the atmospheric and plume temperatures as well as the transmissivities of the pollutant and interfering species in the atmosphere and plume. In principle, it appears that a number of simple radiometric measurements over carefully chosen wavelength intervals and a suitable computer program might be used to obtain quantitative results; however, this is a very complex procedure and not sufficiently accurate. On the other hand, we have devised a technique based upon GFC which is independent of the plume and atmospheric temperatures and which does not require a computer to reduce the data.

The basic components of a single-ended RGFC sensor are shown schematically in Figure 4: a single detector, a light chopper, collecting optics, a gas cell containing the pollutant to be detected, and a reference cell.

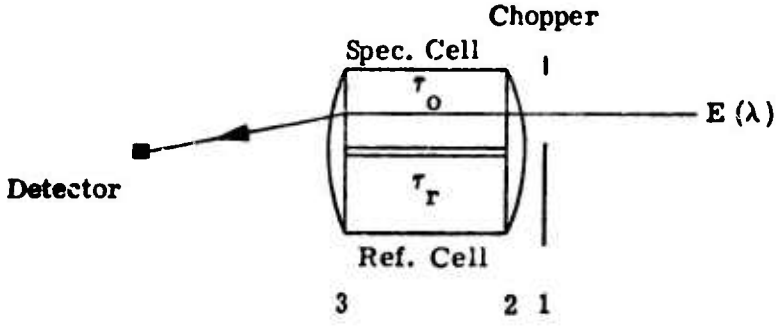

Figure 4. Schematic diagram of remote gas-filter-correlation sensor.

As in the double-ended sensor, the chopper passes the entering radiation alternately between the two cells. When the chopper is in the position indicated in Figure 4, the signal generated at the detector is

$$V_1 = \int_{\Delta\lambda} \{E\tau_2\tau_o\tau_3 + N_1^o\tau_2\tau_r\tau_3 + N_{ins}^o[\epsilon_2(\tau_o\tau_3 + \tau_r\tau_3) + \epsilon_o\tau_3 + \epsilon_3]\} R\,d\lambda \qquad (19)$$

where E is the incoming energy; τ, N^o, and ϵ refer to transmissivity, blackbody function, and emissivity respectively (the numerical subscripts are indicated in Fig. 4, and ins refers to the instrument which is maintained at a constant temperature); and R is the overall responsivity of the detector, optical efficiency, and electronics. All symbols are a function of λ, but for the sake of brevity, this is not noted.

Similarly, when the chopper blocks off the gas cell, the signal generated at the detector is

$$V_2 = \int_{\Delta\lambda} \Big\{ E\,\tau_2\,\tau_r\,\tau_3 + N_1^o\,\tau_2\,\tau_o\,\tau_3 + N_{ins}^o\,[\epsilon_2\,(\tau_o\,\tau_3 + \tau_r\,\tau_3) + \epsilon_r\,\tau_3 + \epsilon_3] \Big\}\, R\,d\lambda \qquad (20)$$

The AC signal generated is the difference between V_2 and V_1:

$$\Delta V = \int_{\Delta\lambda} [\tau_r - \tau_o][\tau_2\,\tau_3(E + N_1^o) - \tau_3\,N_{ins}^o]\,R\,d\lambda \qquad (21)$$

where ϵ has been replaced by $1-\tau$.

The instrument is balanced, or zeroed, with $E = O$, by adjusting the aperture of the reference cell; that is,

$$\int_{\Delta\lambda} \tau_3(\tau_2 N_1^o - N_{ins}^o)\,(\tau_r - \tau_o)\,R\,d\lambda = O \qquad (22)$$

Since R, τ_2, and τ_3 are only slowly varying functions of λ, an overall effective responsivity, R_o, may be defined by $R_o = \overline{\tau_2\,\tau_3\,R}$ where the bar denotes the mean value over the interval $\Delta\lambda$. Thus, when $E \neq O$ the AC signal is given by

$$\frac{\Delta V}{R_o} = \int_{\Delta\lambda} E(\lambda)\,[\tau_r - \tau_o(\lambda)]\,d\lambda \qquad (23)$$

where $E(\lambda)$ is given by Equation 15.

When $E(\lambda)$ is introduced into Equation 23 and the integration over $\Delta\lambda$ carried out, one obtains

$$\frac{\Delta V}{R_o} = \tau_i \overline{N_b^o}' (\bar{\tau}_a - \overline{\tau_a \tau_a}') (\bar{\tau}\tau_r - \overline{\tau\tau}_o)$$

$$+ \overline{N_c^o} [\bar{\tau}_a (\tau_r - \bar{\tau}_o) + \bar{\tau}_a \bar{\tau}_i (\overline{\tau\tau}_o - \bar{\tau}\tau_r)]$$

$$+ \overline{N_b^o} (1 - \bar{\tau}_a)(\tau_r - \bar{\tau}_o) \qquad (24)$$

Since by balancing the instrument, $\bar{\tau}_o = \tau_r$, Equation 17 may be simplified:

$$\frac{\Delta V}{R_o} = \bar{\tau}_i [\bar{\tau}_a \overline{N_c^o} - (\bar{\tau}_a - \overline{\tau_a \tau_a}') \overline{N_b^o}'] (\overline{\tau\tau}_o - \bar{\tau}\tau_r) \qquad (25)$$

Thus, an expression results that shows the AC signal is effectively a product of a modulation function that is only related to the pollutant transmissivity and fixed-instrument transmissivities and of the difference between the radiance emitted by the plume and background atmosphere.

If we now consider a second cell pair with $\bar{\tau}_o' \neq \bar{\tau}_o$, and chopped at a different frequency but using the same detector and optical components, a similar expression is derived:

$$\frac{\Delta V'}{R_o} = \bar{\tau}_i [\bar{\tau}_a \overline{N_c^o} - (\bar{\tau}_a - \overline{\tau_a \tau_a}') \overline{N_b^o}'] (\overline{\tau\tau}_o' - \bar{\tau}\tau_r') \qquad (26)$$

The modulation function has a different response from that given in Equation 25. The different modulation function responses are nonlinear with pollutant concentration and have been shown to be adjustable over a large range (1-3, 6, 7) by varying the amount of pollutant placed in the specifying cell.

Division of Equation 25 by Equation 26 gives

$$\frac{\Delta V}{\Delta V'} = \frac{\overline{\tau\tau}_o - \bar{\tau}\bar{\tau}_r}{\overline{\tau\tau}'_o - \bar{\tau}\bar{\tau}'_r} \tag{27}$$

which is almost completely independent of plume radiance, atmospheric radiance, intervening atmospheric transmissivity, and instrument spectral responsivity.

This technique has been demonstrated both in the laboratory and in the field (1, 2). Remote sensing data were in agreement with extractive data within 25%.

SPECTROMETER DESIGN

General Description

The GFC technique is based upon the existence of a pronounced spectral structure of the gas to be detected. In this respect both HCl and HF are extremely well suited. They possess a rotational fine structure with line spacing to line half-width ratios that exceed 200. Thus, the technique provides high sensitivity (large modulation function) and high specificity (discrimination in the presence of interfering species).

Band spectra of HCl, HF, and some possible interfering species have been generated; the latest, most reliable data are presented in Figure 5. From this figure it is clear that if the HF measurements are confined between 3950 and 4150 cm^{-1} (i.e., $\lambda_o \approx 2.47$ μm and HBW* ≈ 0.12 μm), there will be no interferences except for H_2O. However, if HCl is measured between 2900 and 3000 cm^{-1} (i.e., $\lambda_o \approx 3.39$ μm and HBW ≈ 0.12 μm), some interference may be generated by the presence of NO_2, O_3, NH_3, and CH_4.

The detailed design of the GFC spectrometer is described in the System/Equipment Manual. Thus, only a brief description is presented here.

---

* Optical filters' half bandwidth.

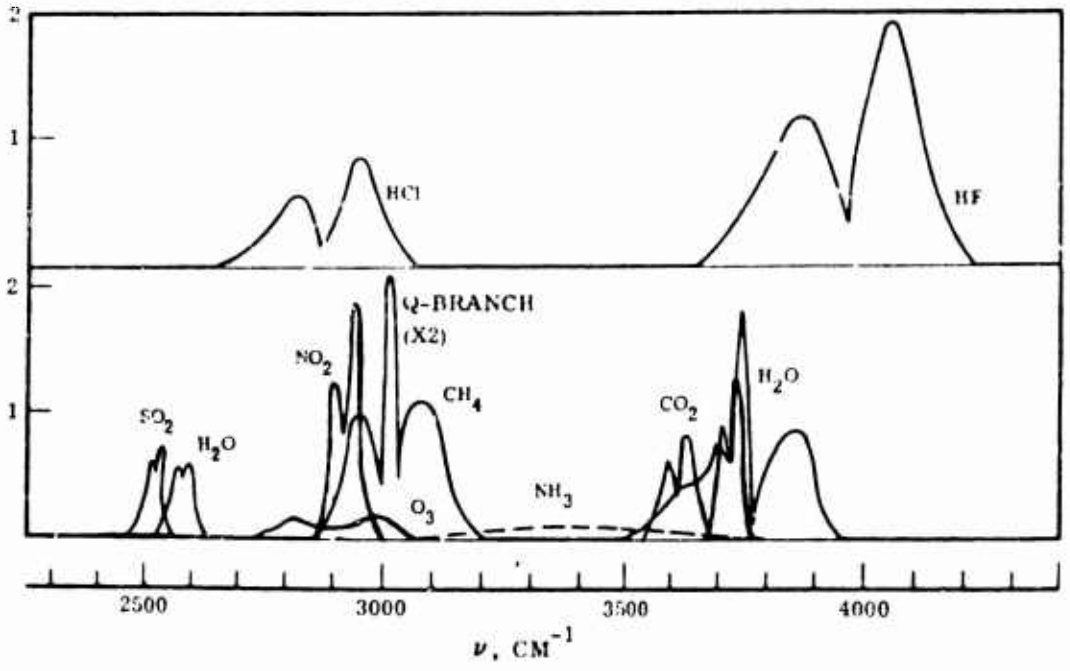

Figure 5. Band spectra of HCl, HF, and interfering species.

Figure 6 is a schematic drawing of the optical system. The optical system consists of a source aperture which is imaged by the source lens onto the detector lens, and a detector lens which images the source lens (cell mask) onto the detector.

High-frequency cell chopping (ΔV) is performed by a tuning-fork chopper at 200 Hz, and the low-frequency source chopping (V) at 12.6 Hz by a rotating chopper with a mirrored surface facing the source. This reduces the effects of temperature changes of the chopper blade on the V signal. Both choppers are located at the source end of the instrument to minimize the number of components with chopped emission. The design slightly modifies the theoretical expressions in that, with the relative positioning of the two choppers, there is no high-frequency component during phase P′ (see Fig. 2). This reduces the electronics circuitry requirements.

The lenses are both IR-2 positive meniscus lenses, 2.54 cm in diameter. Since IR-2 material has a relatively constant index of refraction (2.25 for wavelengths between 2.5 and 3.5 μm), no shift in focus will occur when changing from HCl to HF. Only the gas-cell assembly and optical filter need to be changed to convert from one gas to the other. Details are given in the System/Equipment Manual.

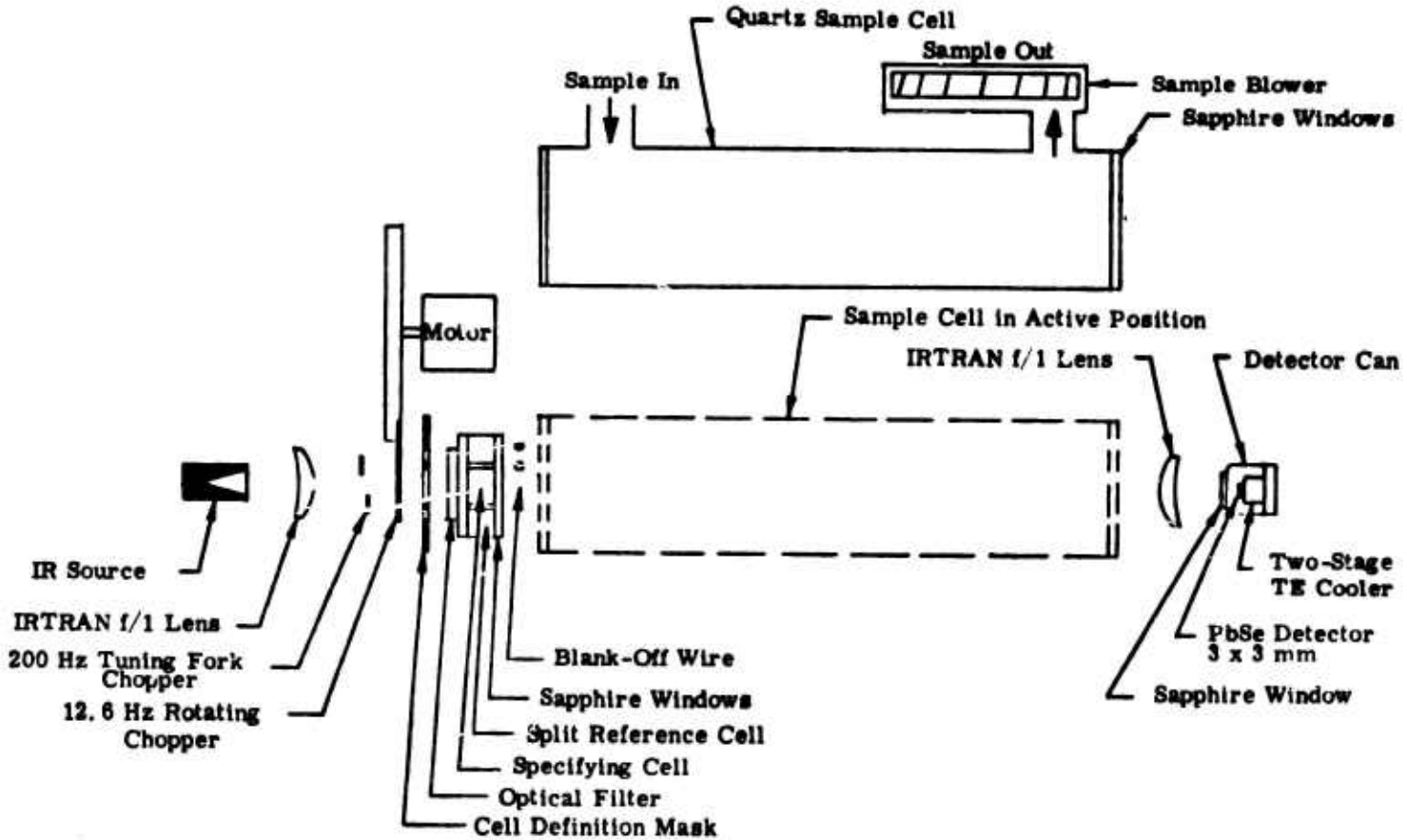

Figure 6. Optical system schematic.

The source aperture required is about 3 mm; this is oversized to accommodate any slight motion due to thermal expansion of the support structure near the high-temperature source. The source requires about 25 W to achieve a 1050°K temperature.

The detector (3 x 3 mm, PbSe) is located on a two-stage thermoelectric cooler to achieve an operating temperature of 280°K and is temperature regulated to 0.3°K. The high degree of regulation minimizes responsivity changes during operation.

The quartz sample cell is 20 cm long and may be removed for true in-situ operation.

A blank-off wire can be inserted into the reference cell field of view. This provides for a span reference calibration by mechanically creating a fixed reproducible offset in the ΔV signal. Zeroing is done electronically.

Figure 7 gives a simplified block diagram of the electronics system used in the unit. Infrared radiation chopped at two frequencies, f_1 (200-Hz cell chopper) and f_2 (12.6-Hz source chopper), falls upon the temperature-stabilized PbSe detector. The output of the detector is amplified with a low-noise preamplification and additional stages of amplification, and then is split into inputs to the ΔV and V channels.

The ΔV input is passed through a bandpass filter to remove the f_2 component of the signal. The output of the filter is then fed to span and range amplifiers which respectively adjust the magnitude of the signal for full-scale span and measuring range on the instrument output. The output of the range amplifier is fed into four, gated sample and hold systems, which sample different but specific parts of the input signal according to triggering inputs from the data gates.

The gating system controls those portions of the ΔV and V channel inputs that are fed to the various sample and hold systems; it receives sync signals from both source and cell choppers. The sync pulses from the choppers are shaped and amplified and then fed to the width, phase, and sync adjust systems. These systems allow adjustments of the various gate commands.

The outputs of the unit are ΔV, V, and $\Delta V/V$, where the ΔV V signal is derived by applying the ΔV and V signals to an analog divider. The display is a panel meter, and a jack for a strip-chart recorder is provided.

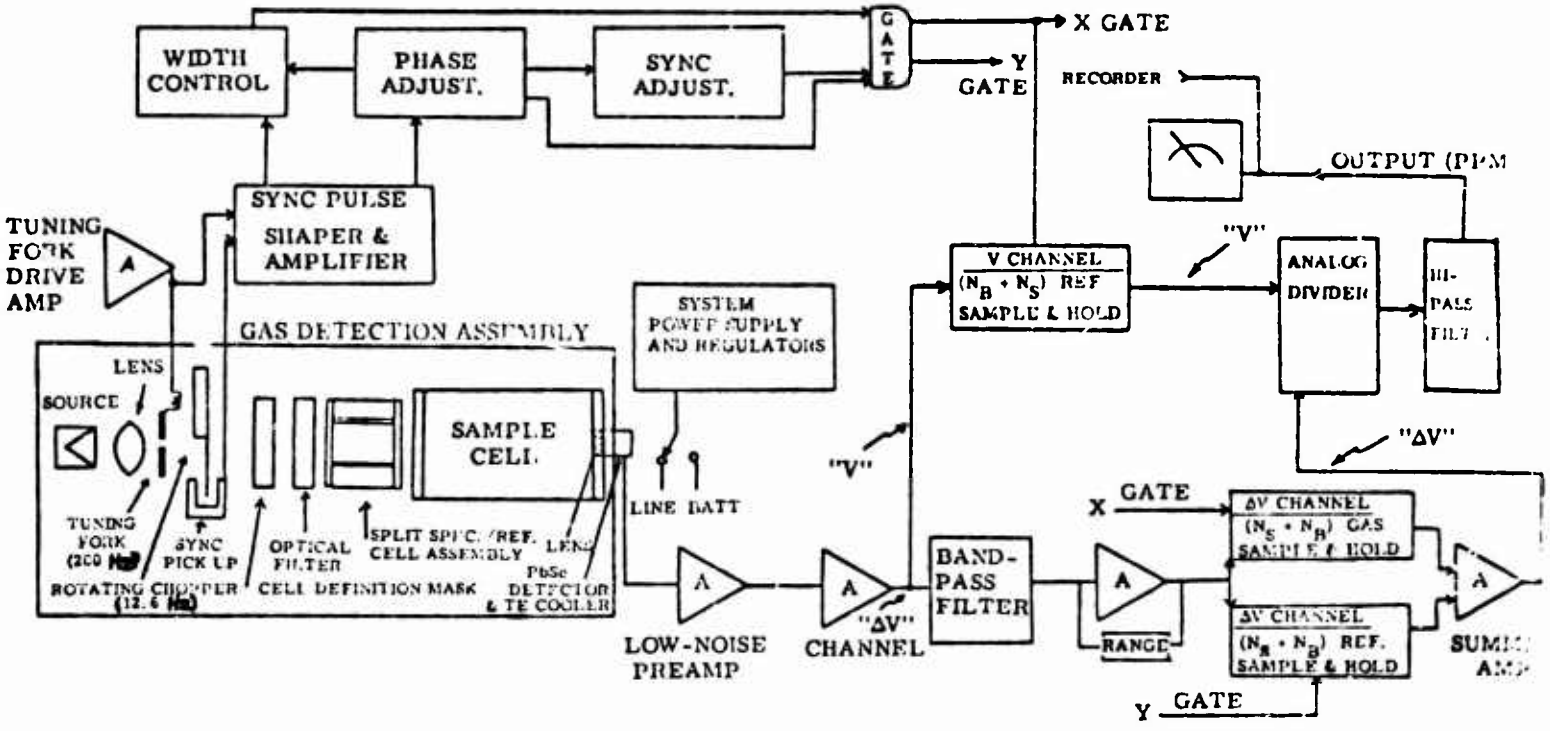

Figure 7. Block diagram of GFC spectrometer electronics system.

Design Performance

The minimum detectable signal for the instrument is given by

$$S = \Delta V = \eta A \Omega N^{O} \tau_{O} \bar{k} C L p \Delta\lambda R, \text{ volts} \qquad (28)$$

where

η	is the overall efficiency
A	is the area of the specifying cell
Ω	is the source solid angle
N^{O}	is the blackbody source radiance
τ_{O}	is the specifying-cell transmissivity
$\bar{k}$	is the absorption coefficient
C	is the concentration
L	is the optical pathlength
p	is the sample pressure
$\Delta\lambda$	is the filter HBW
R	is the detector responsivity

For a detector-noise limited system, the root mean square (rms) noise is

$$N_{rms} = \frac{\sqrt{A_d \Delta f}}{D^*} R, \text{ volts} \qquad (29)$$

where

A_d	is the detector area
Δf	is the electronics-noise bandpass
D^*	is the detectivity
R	is the detector responsivity

The values of the instrument parameters for measuring HCl and HF are presented in Table 1.

TABLE 1. SUMMARY OF INSTRUMENT PARAMETERS

Parameter	HCl	HF	Note
η	0.031	0.031	a
A, cm^2	2.16	2.16	--
Ω, sr	0.012	0.012	b
N^0(T = 1050°K, W/cm^2-μ-sr	0.47	0.51	c
τ_0	0.81	0.90	d
$\bar{k}$, $atm^{-1}cm^{-1}$	0.50	0.75	e
L, cm	20.0	20.0	--
P, atm	1.0	1.0	--
$\Delta\lambda$, μm	0.18	0.11	f
R, V W	1.05×10^4	1.05×10^4	g
A_d, cm^2	0.09	0.09	--
Δf, Hz	0.025	0.025	h
D*, cm $H^{1/2}$ W	2.0×10^9	1.7×10^9	i
S (C = 1), V	5.76	6.39	--
N_{rms}, V	2.5×10^{-7}	2.9×10^{-7}	--
C_{min}	43 ppb	46 ppb	j

[a] η is assumed to be the product of the transmissivities of the two lenses (τ_L), the two cell windows (τ_W), the two sample-cell windows (τ_S), the gas transmissivity (τ_G), the emissivity of the source (ϵ_S), the optical filter (τ_F), and the electronics efficiency (η_e); viz

$$\begin{aligned} \eta &= (\tau_L)^2 (\tau_W)^2 (\tau_S)^2 (\tau_G) (\epsilon_S) (\tau_F) (\eta_E) \\ &= (.75)^2 (.88)^2 (.88)^2 (.9) (.5) (.65) (.31) \qquad (30) \\ &= .031 \end{aligned}$$

[b] $\Omega = \pi \sin^2\alpha \approx \pi \left(\frac{1.25}{20}\right)^2$

[c] For HCl, $\lambda_0 = 3.4$ μm, and for HF, $\lambda_0 = 2.5$ μm.

[d] Based on measured values with the pertinent optical filters.

[e] Same as note d.

[f] Uses actual optical filter HBW.

[g] Actual measured responsivity of the detector at operating temperature of 20°C; this value differs from the detector data sheet shown in the System/Equipment Manual.

[h] $\Delta f = 1/4t$ where t is the time constant to reach 90% of full scale (= 10 seconds).

[i] Actual detector D* at 200 Hz and T = 20°C; this value differs from the detector data sheet shown in the System/Equipment Manual.

[j] C_{min} is minimum detectable concentration for S N_{rms} = 1.

From the instrument parameter values given in Table 1 and Equations 29 and 30, it is calculated that the minimum detectabilities for HCl and HF are 43 and 46 ppb, respectively. If, however, the minimum detectability is defined by $S/N_{p-p} = 1$, where N_{p-p} is the peak-to-peak noise, the minimum detectabilities will be higher by a factor of 5.

Conversion to Long-Path Operation

Figure 8 shows the conversion technique for operating the unit as a long-path instrument. The sample cell is removed and replaced with a beam-splitting pellicle. For optimum performance the pellicle should be ~66% reflecting. The source beam is diverted by the beam splitter to the retroreflector. The retroreflector, recently developed, is an array of corner cubes which is noncritical in alignment. The reflected rays retrace the incident ray except for a displacement that depends on the corner-cube dimension of the retroreflector. The beam spread is thereby minimized.

The return beam from the retroreflector is partially transmitted through the pellicle and reflected by the flat mirror and beam splitter onto the collecting optics. The optical efficiency (0.15) of the two reflections and one transmission through the beam splitter results in a beam-intensity reduction. The rays that pass straight through the beam splitter to the detector will create some modulation; however, since this optical path is only 10 cm, its contribution to the signal is negligible compared to the signal generated over long optical paths.

When this adaptation is implemented, the system's performance depends on the optical range, R, at which the retroreflector is placed and its physical size, D_R. The system would be perfectly matched if

$$\frac{D_R}{R} = \frac{D_S}{f} \tag{31}$$

where D_S is the source diameter (0.3 cm) and f is the focal length of the source lens (2.54 cm). Thus, for operation at a range of 500 m (optical path equal to 1 km)

$$D_R = 500 \left(\frac{0.33}{2.54}\right) = 50 \text{ m}$$

This is clearly impractical.

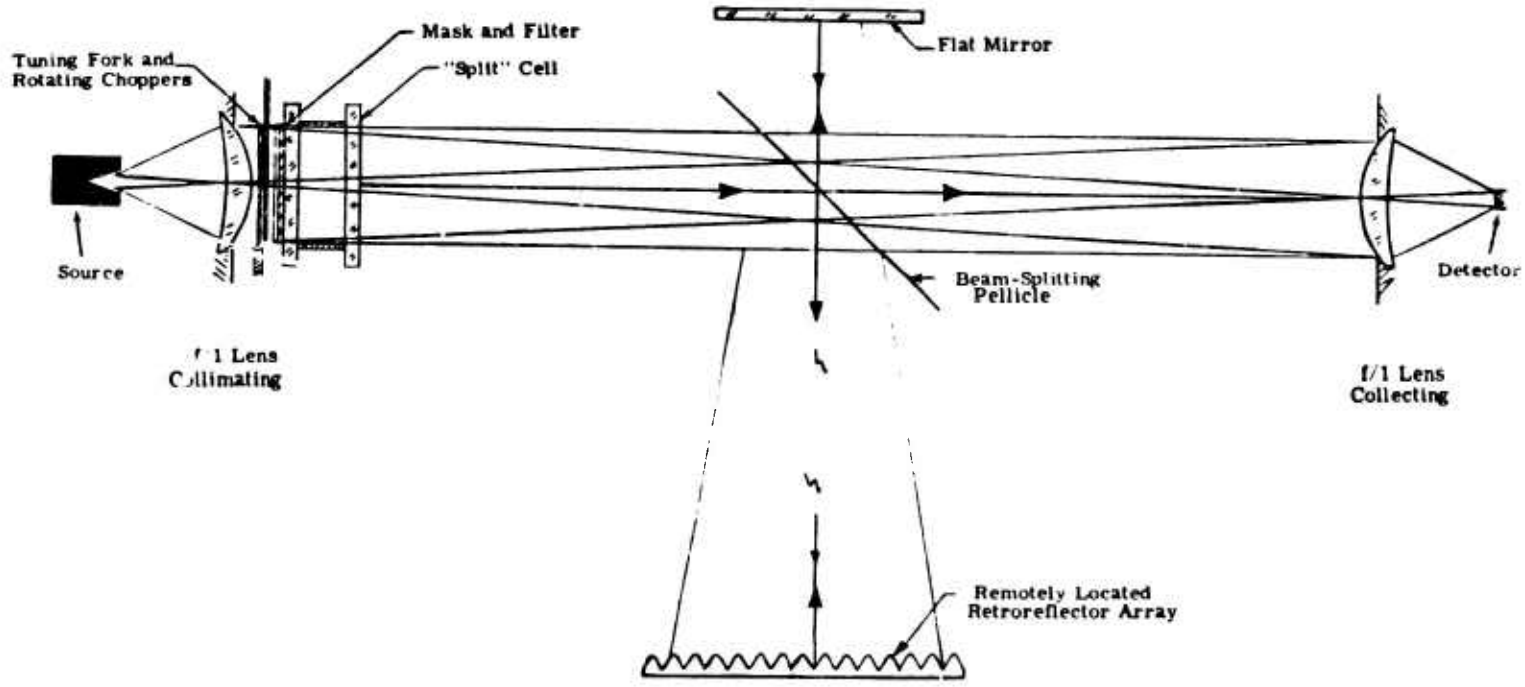

Figure 8. Extended path of GFC schematic.

Practically, 1- to 2-m retroreflectors can be constructed, and adequate sensitivities can still be obtained as illustrated in the following. The sensitivity, S, is proportional to the solid angle subtended by the retroreflector, Ω_R, times twice the range (2R); viz

$$S \propto \Omega_R (2R) \tag{32}$$

and, by definition

$$\Omega_R \approx \pi (D_R/2R) \tag{33}$$

for small solid angle. Then, the sensitivity ratio, S. R. (i. e., the sensitivity of the spectrometer operating as a long-path system divided by the sensitivity of the spectrometer operating in its normal mode over a 20-cm optical path), is given by

$$\text{S. R.} = \frac{\pi D_R^2/2R}{0.2\,\Omega} \times \eta \tag{34}$$

where $\Omega = 0.012$ sr (see Table 1), and $\eta (= 0.15)$ is the resulting loss in optical transmissivity. Equation 34 only applies for ranges equal to or greater than the range calculated by Equation 31; this is the point where the beam divergence is equal to D_R. For shorter ranges, the S. R. decreases linearly with range. This effect is shown in Figure 9 for 1- and 2-m retroreflectors.

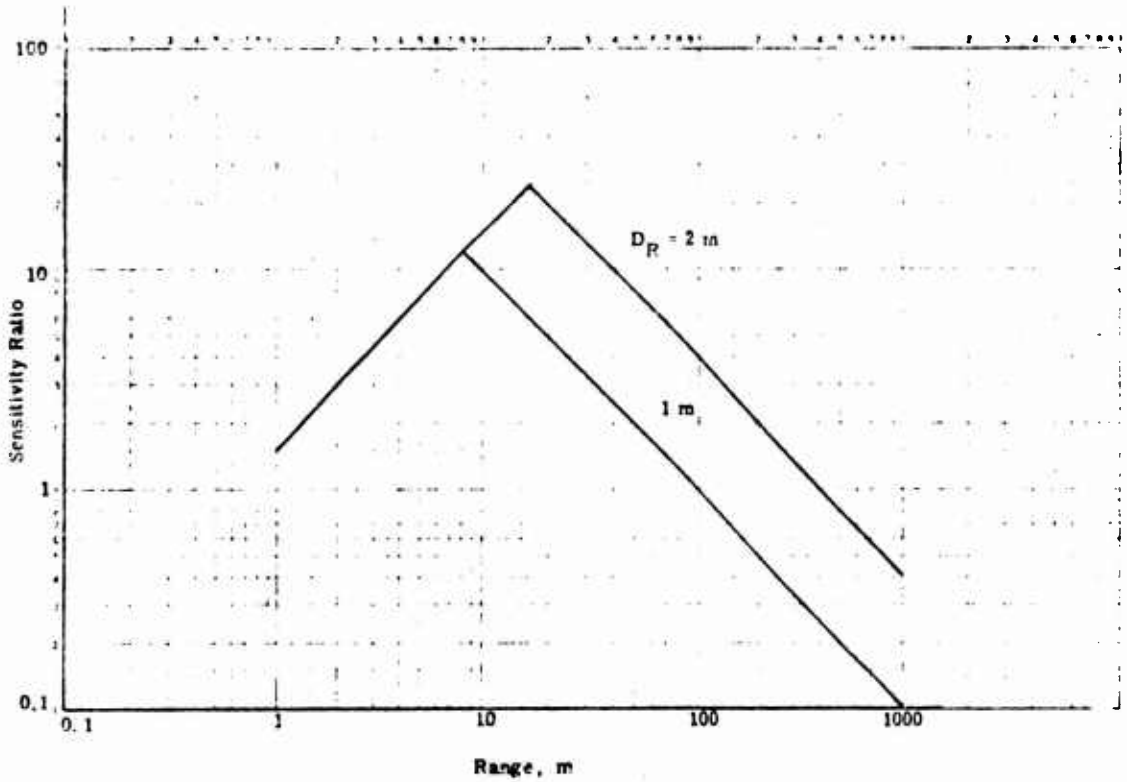

Figure 9. Sensitivity of system operating in long-path mode compared with sensitivity of spectrometer.

LABORATORY STUDIES

HCl Experiments

Optimization--Previous laboratory studies (3) have shown that an optimum value exists for the specifying cell's optical thickness, u_o, or transmissivity, τ_o. However, this depends on the exact spectral characteristic of the optical filter used. The spectral transmission for the HCl filter is presented in Figure 10; superimposed on the figure is the average absorption coefficient, $\bar{k}$. The R-branch of the HCl absorption spectrum is seen to be almost precisely centered.

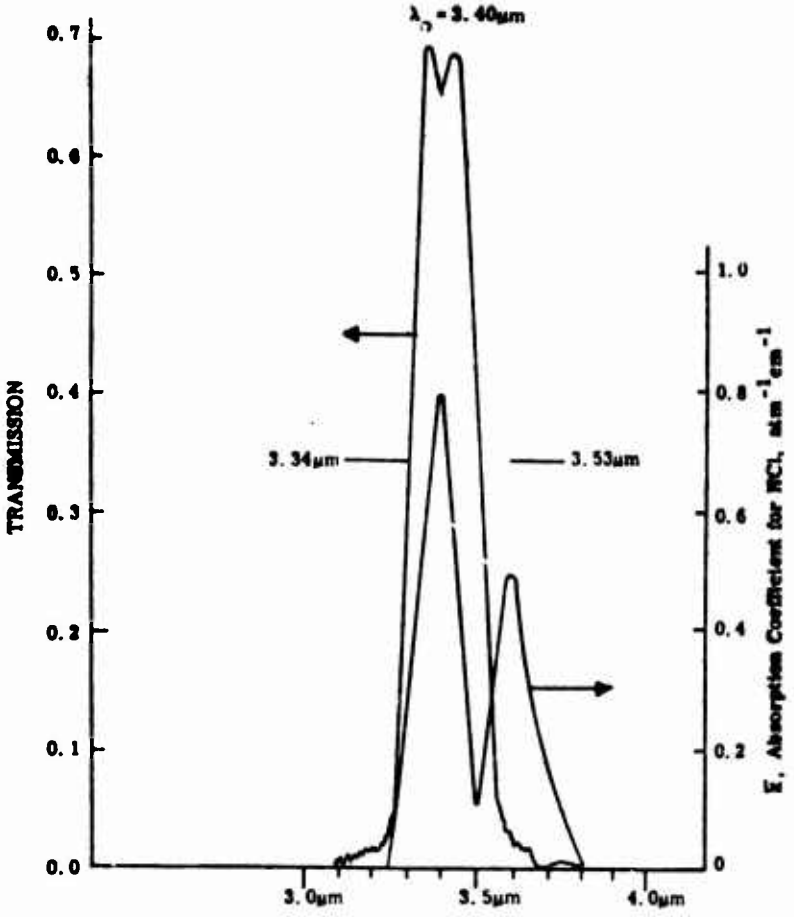

Figure 10. Spectral characteristics of HCl filter and HCl absorptivity.

Transmission measurements of HCl were made using the filter and a 1-cm cell; the results are summarized in Table 2.

TABLE 2. EXPERIMENTAL MEASUREMENTS OF HCl ABSORPTION

u_o, atm-cm	τ_o, %	$\bar{k}$, $atm^{-1}cm^{-1}$
0.5[a]	89.5	0.55
1.0	81.4	0.52
1.5	73.0	0.54

[a] Pressurized to 1 atm with N_2.

It has been shown (5) that a good representation of the curve of growth for a homogeneous gas mixture is given by

$$\bar{\tau} = \exp[-\bar{k}u(1 + ku/4a_o p_e)^{-1/2}] \quad (35)$$

where a_o is the ratio of line half-width to line spacing (= 0.003) and p_e is the equivalent pressure given by

$$p_e = p_G B + p_N = p_t[C(B-1) + 1] \quad (36)$$

with p_G and p_N representing the partial pressures of gas and nitrogen, respectively, and B the ratio of self-broadening to nitrogen-broadening efficiency (≈ 8). Using Equations 35 and 36, the average $\bar{k}$'s for three experiments were calculated (Table 2).

Measurements were made of the relative signal, using 100 ppm HCl diluted with N_2 to 1 atm pressure in the sample cell with varying u_o. These data are presented in Figure 11 along with data from previous studies (3). These results indicate that the optimum τ_o is about 0.8. This corresponds to u_o = 1 atm-cm (Table 2).

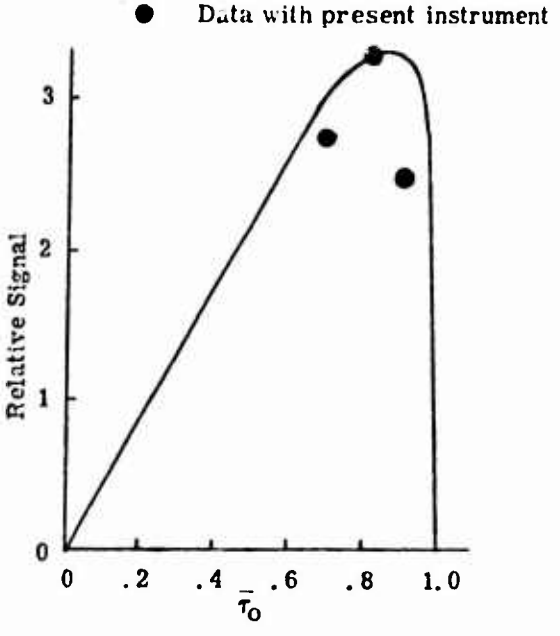

Figure 11. Relative signal as a function of HCl transmissivity (3).

Sensitivity--The instrument was calibrated by using N_2-diluted mixtures of HCl pressurized to 1 atm pressure over a concentration range of 1- to 1000-ppm HCl. Test gas mixtures were placed in the sample cell alternately with samples of pure N_2 at 1 atm. A composite of the final test records is shown in Figure 12; from this, data are compared, in terms of signal and noise, with the theoretical predictions.

For the 10-ppm case, the observed signal is 2.4 V on the x 1 scale. Referring to the System/Equipment Manual, the total electronic gain is 44,000 (on the x 1 scale). Thus, at the detector the observed signal is 2.4/44,000 (5.5×10^{-5}V), compared with the theoretically calculated signal of 5.8×10^{-5}V (Table 1).

Also for the 10-ppm case, the observed peak-to-peak noise is about 0.2 V (4.5×10^{-6}V) at the detector. In terms of rms noise, this is equivalent to $9 \times 10^{-7} V_{rms}$ using a factor of 5 to convert peak-to-peak random noise to rms noise; i.e., 99% of the noise energy exists within a voltage range of $5 \times V_{rms}$. This value is higher by a factor of 3.6 than that calculated in Table 1.

Since the signal-to-noise ratio is linear from 10 ppm to lesser concentrations, the data indicate a threshold sensitivity ($S/N_{rms} = 1$) of 167 ppb. A calibration curve is given in the System/Equipment Manual.

Specificity--From examination of the absorption band spectra presented in Figure 5, only CH_4, NH_3, and NO_2 should impair the specificity of HCl measurements (ambient O_3 concentrations should be so low as to have no effect). The effects of these three species were measured; sample test results are shown in Figure 12. Additional data were taken at other concentrations, and the results are presented graphically in Figure 13 in terms of equivalent HCl (NO_2 and NH_3 give a negative signal, and CH_4 a positive).

A numerical discrimination ratio (D. R.) can be defined as the ratio of the concentrations of the interfering species to the equivalent HCl concentration. These are presented in Table 3.

Specificity experiments were conducted using ambient air saturated with H_2O (100% relative humidity). Within the noise level of the instrument, no signals were observed.

These results indicate the high specificity obtained using the GFC technique.

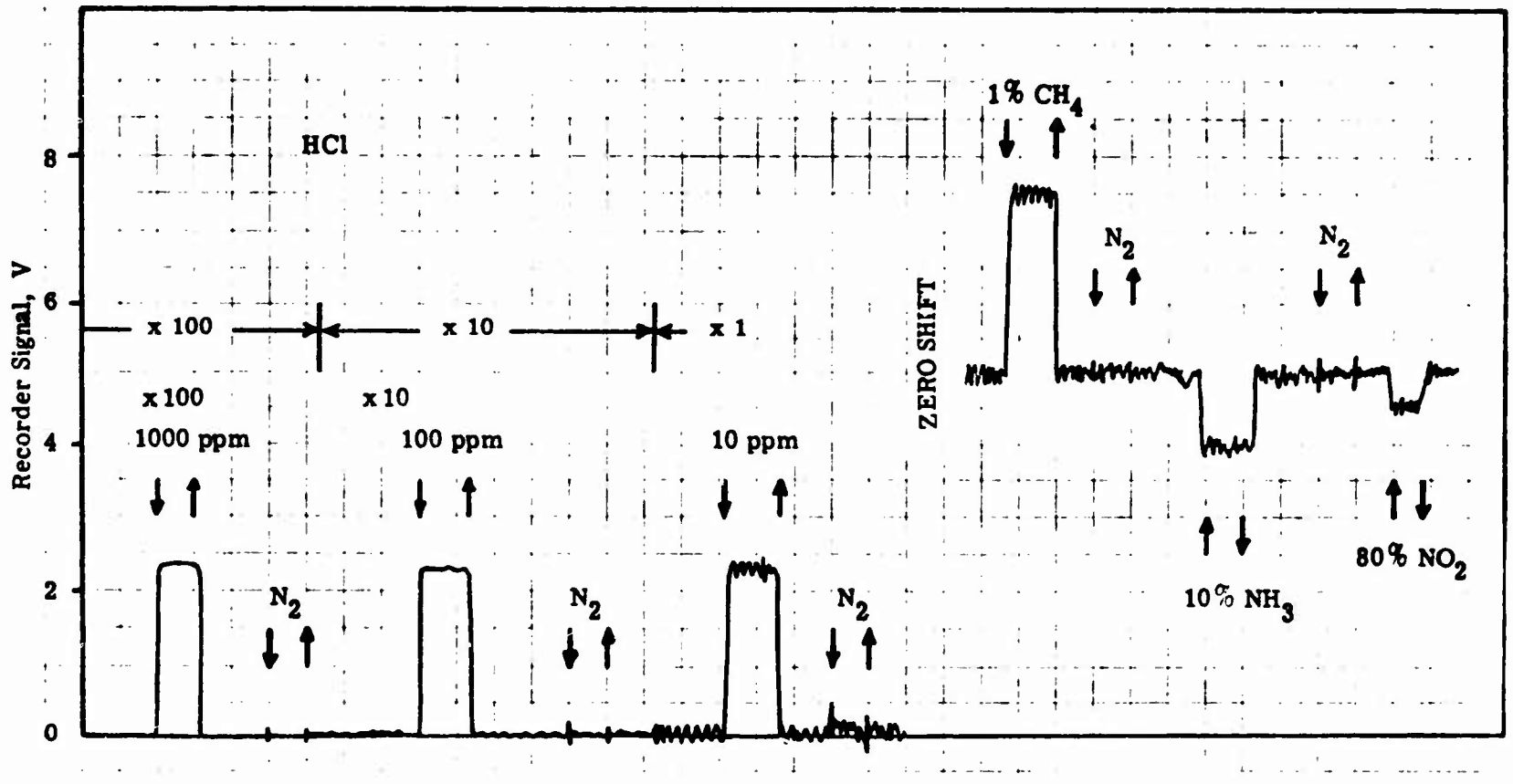

Figure 12. Composite tracing of laboratory calibration results.

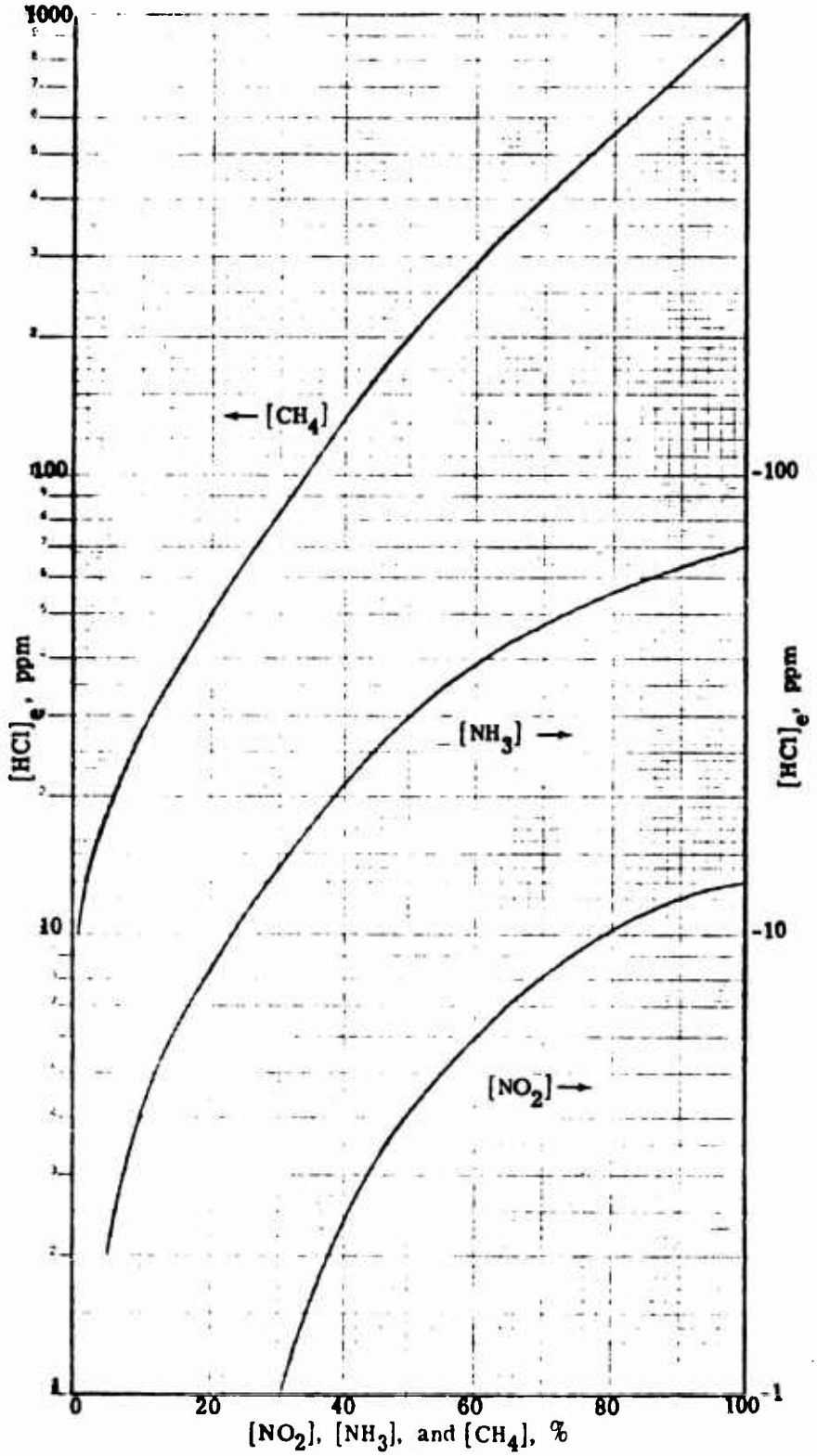

Figure 13. HCl specificity test results.

TABLE 3. HCl DISCRIMINATION RATIO FOR CH_4, NH_3, AND NO_2

Species	Concentration (%)	D. R.
CH_4	100	10^3
	50	2.5×10^3
	10	3.7×10^3
	1	10^3
NH_3	100	-1.7×10^4
	50	-1.7×10^4
	10	-2.5×10^4
NO_2	100	-7.7×10^4
	50	-1.2×10^5

HF Experiments

Optimization--Laboratory experiments similar to those for HCl were conducted for HF. The spectral transmission of the HF filter and its average absorption coefficients are presented in Figure 14; transmission measurement data, in Table 4.

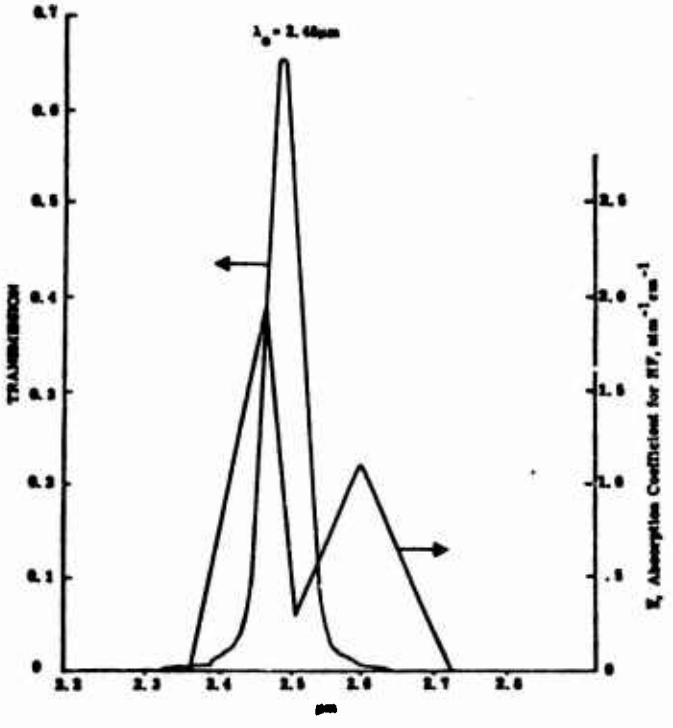

Figure 14. Spectral characteristics of HF filter and HF absorptivity.

TABLE 4. EXPERIMENTAL MEASUREMENTS OF HF ABSORPTION

u_o, atm-cm	τ_o, %	$\bar{k}$, $atm^{-1}cm^{-1}$
0.5[a]	90	0.76
1.0	83	0.75

[a] Pressurized to 1 atm with N_2.

As in the case of HCl, the average absorption coefficients were calculated using Equations 35 and 36, assuming $a_o = 0.0015$ and $B = 8$.

Measurements were made of the relative signal, using 100 ppm HF diluted with N_2 to 1 atm pressure in the sample cell with $u_o = 0.5$ and 1 atm-cm. The data are shown in Figure 15, along with data from previous studies (3). A specifying-cell optical thickness of 0.5 atm-cm was selected as the optimum value.

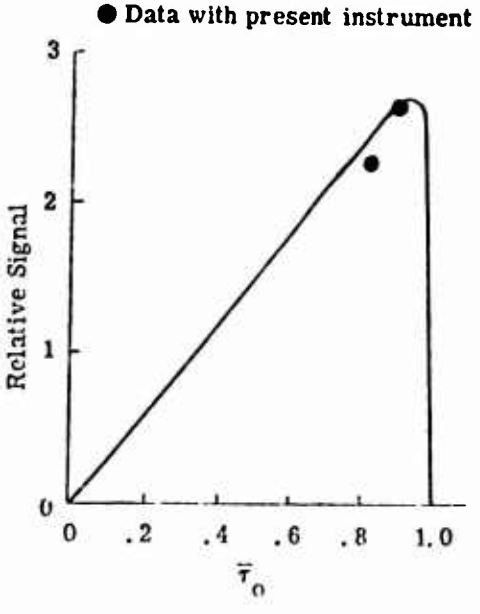

Figure 15. Relative signal as a function of HF transmissivity (3).

Sensitivity--Calibrating the monitor for N_2-diluted HF by mixing test gas mixtures based upon partial-pressure measurements was a difficult task due to the highly adsorptive nature of HF coupled with its high boiling point (19.8°C). This was established during previous studies (3), which showed that large uncertainties arise for HF concentrations below

about 5000 ppm. By applying the correction factors used previously, reliable data were obtained over the concentration range of 100 to 1000 ppm. The calibration curve is given in the System/Equipment Manual.

Measurements of the signal and noise for [HF] = 100 ppm are 20 and 0.2 V_{p-p}, respectively (normalized to the x1 scale). In terms of the theoretical values given in Table 1, the observed signal is 4.5×10^{-4}V compared with 6.4×10^{-4}V, and the observed rms noise is 9.1×10^{-7} compared with 2.9×10^{-7}V. These data indicate a threshold sensitivity of 200 ppb.

Specificity--The only species likely to create an interference problem is H_2O. Although previous studies had indicated some interference due to NH_3, for this system no signal was observed when 100% NH_3 at 1 atm pressure was admitted to the sample cell. Laboratory air and water vapor were measured. Results are presented in Figure 16 and show that discrimination ratios greater than 10^5 are achieved.

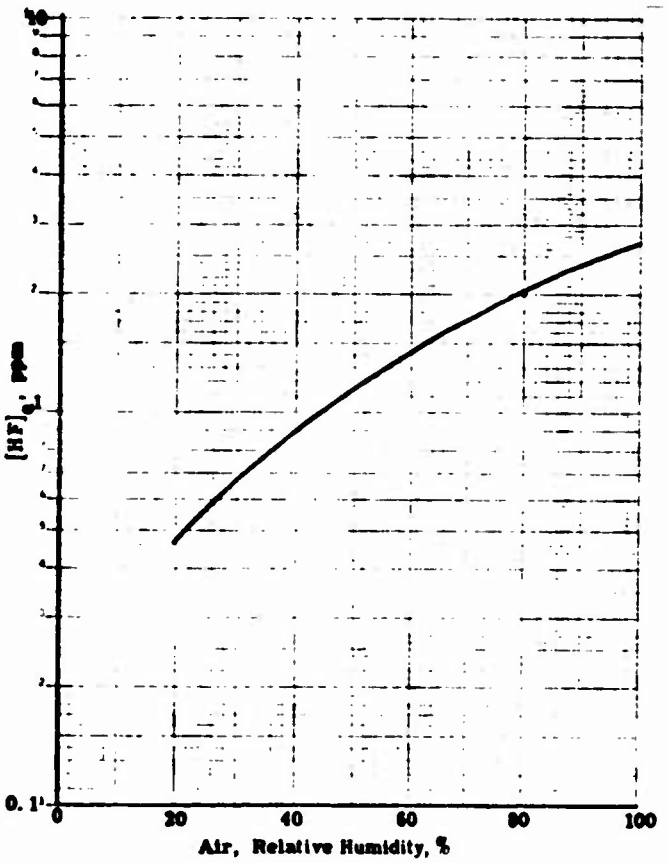

Figure 16. HF specificity test results

DISCUSSION

The prototype field instrument has been tested in the laboratory. Threshold sensitivities of 167 and 200 ppb for HCl and HF, respectively, were determined. The GFC technique provided excellent specificity in the presence of interfering species. However, several drawbacks exist with the prototype. These are:

(1) The sensitivities are about a factor of 5 higher than predicted from theoretical considerations, mainly because of excess noise that occurs at a relatively low frequency (~0.02 Hz). This noise is due to a random coupling of the 200 and 12.6 Hz choppers, occasionally generating a resonance beat. A revised chopping system would eliminate this problem.

(2) The infrared source designed for this system exhibits significant spatial nonuniformities. This generally results in a relatively long warm-up time before its temperature uniformity is stabilized, and the ratioing technique eliminates source dependencies. A new, higher temperature, fast stabilizing, uniform source has recently been developed, but incorporating it into the present system was not feasible because of lack of time and funding.

(3) Wall adsorption effects, particularly when measuring HF, cause severe problems when the system is used in the sampling mode. Operation in the in-situ mode apparently would give the best results.

(4) Movement of the sample cell during operation creates some internal reflections and may give an apparent signal. A more positive positioning device should be incorporated.

(5) The transmissivity of the HF in the specifying cell is temperature dependent because of wall adsorption. If operated below 20°C or over 30°C, the monitor may give erroneous readings unless it is calibrated at its operating temperature. An alternative solution would be to temperature regulate the specifying cell.

(6) The sensitivity to HF is worse than to HCl because of the optical filter used. An ideal filter that matches the spectral absorption of HF is difficult to obtain without paying an exorbitant price.

CONCLUSIONS AND RECOMMENDATIONS

A portable GFC spectrometer has been developed to continuously monitor HCl and HF over the concentration range of 1 to 1000 ppm. The unit uses either 115 VAC 60 Hz or 12 VDC. Attained threshold sensitivities of 167 and 200 ppb for HCl and HF, respectively, are nearly those predicted from theoretical considerations. Excellent specificity is obtained in the presence of anticipated interfering species. The system also has the potential of being converted into a long-path (~ 1 km) sensor with about the same sensitivities. A technique for passive single-ended remote sensing is described that appears to offer significant potential.

It is recommended that--

(1) A new system be developed that eliminates the drawbacks enumerated in the Discussion section.

(2) The system be equipped with additional optics needed to permit operation over long, horizontal optical paths.

(3) The system be developed to permit single-ended remote sensing.

ACKNOWLEDGMENTS

The valuable assistance of L. L. Acton, D. P. Ferreira, G. D. Hall, P. R. Heid, G. K. Houghton, and E. A. Meckstroth in the design, fabrication, and testing of the spectrometer is gratefully acknowledged.

REFERENCES

1. Bartle, E. R. Comparison of remote sensing and extractive techniques for measuring SO_2 concentrations emitted by a coal burning power plant. Final report, EPA contract 68-02-1481, October 1974.

2. Bartle, E. R. Infrared sensor for the remote monitoring of SO_2. Interim report, EPA contract 68-02-1208, April 1974.

3. Bartle, E. R., et al. An in-situ monitor for HCl and HF. J Spacecraft and Rockets 9:836 (1972).

4. Chandrasekhar, S. Radiative transfer. New York: Dover Publications, Inc., 1950.

5. Ludwig, C. B., et al. Study of air pollutant detection by remote sensors. NASA report CR-1380, July 1969.

6. Ludwig, C. B., et al. Remote measurements of air pollution by nondispersive optical correlation. AIAA paper 71-1107, presented at Joint Conference on Sensing of Environmental Pollutants sponsored by ACS, AIAA, EPA, IEEE, ISA, NASA, and NOAA. Palo Alto, California, November 1971.

7. Ludwig, C. B., et al. Air pollution measurements from satellites. NASA report CR-2324, November 1973.

8. Luft, K. F. Über eine neue Methode der registrierenden Gasanalyse mit Hilfe der Absorption ultraroter Strahlen ohne spektrale Zerlegung. Z Techn Phys 24:97 (1943).

9. Maugh, T. H., II. Air pollution instrumentation: A trend toward physical methods. Science 177:685 (1972).

10. Maugh, T. H., II. Air pollution instrumentation (II): The glamour of lasers. Science 177:1090 (1972).

11. Wright, N., and L. W. Herscher. Recording infrared analyzers for butadiene and styrene plant streams. JOSA 36:195 (1946).